Available online at www.sciencedirect.com
ScienceDirect
Journal of Catalysis 255 (2008) 114–126
JOURNAL OF CATALYSIS
www.elsevier.com/locate/jcat

Oxidation of propane to propylene oxide on gold catalysts

Juan J. Bravo-Suárez [a], Kyoko K. Bando [a], Jiqing Lu [a,b], Tadahiro Fujitani [a], S. Ted Oyama [a,c,*]

[a] Research Institute for Innovation in Sustainable Chemistry, National Institute of Advanced Industrial Science and Technology, AIST Tsukuba West, 16-1 Onogawa, Tsukuba, Ibaraki 305-8569, Japan

[b] Zhejiang Key Laboratory for Reactive Chemistry on Solid Surfaces, Institute of Physical Chemistry, Zhejiang Normal University, Jinhua 321004, China

[c] Environmental Catalysis and Nanomaterials Laboratory, Department of Chemical Engineering (0211), Virginia Polytechnic Institute and State University, Blacksburg, VA 24061, USA

Received 3 January 2008; revised 29 January 2008; accepted 30 January 2008

Abstract

Propane epoxidation was carried out by sequential propane dehydrogenation–propylene epoxidation steps using a two-catalyst bed and H_2 and O_2 as the oxidant mixture. The propane dehydrogenation step used a Au/TiO_2 catalyst that was active at the low temperature (443 K) used for the propylene epoxidation step; the latter used a Au/TS-1 catalyst. In situ Au L_3-edge X-ray absorption near-edge structure and ultraviolet–visible measurements on Au/TiO_2 under propane dehydrogenation conditions showed activation of oxygen on gold nanoparticles and evidence for the formation of adsorbed oxygen intermediate species responsible for the production of propylene. Propane epoxidation with H_2 and O_2 at 443 K and 0.1 MPa with the dual Au/TiO_2 and Au/TS-1 catalysts resulted in an overall propane conversion of 2%, propylene selectivity of 57%, and propylene oxide selectivity of 8%, corresponding to a propylene oxide space-time yield of 4 $g\,kg_{cat}^{-1}\,h^{-1}$. The catalysts showed little deactivation and maintained their conversion and selectivity levels for the 12 h duration of the measurements.

Keywords: Gold; Titania; TS-1; Propane; Oxidative dehydrogenation; Propylene; Epoxidation; Propylene oxide; In situ UV–vis; In situ X-ray absorption spectroscopy

1. Introduction

The selective oxidation of low-cost, abundant light alkanes, such as methane, ethane, and propane, is a major academic and industrial research challenge. In the case of propane, significant advances have been attained in the liquid and gas phases for its catalytic oxidation to different products, including propylene [1–3], acetone [4–8], 2-propanol [4,5,8,9], acrylic acid [10–13], acrolein [12,14], acetic acid [10,12], and formaldehyde [15]. In the liquid phase, propane selective oxidation is typically carried out at temperatures below 373 K with oxygen (at high pressures), hydrogen peroxide, or organic hydroperoxides as the oxidants and biomimetic complexes (e.g., Fe, Co, Cu, or Mn porphyrins, phthalocyanines, and polyoxometalates) or Ti-, V-, or Fe-containing materials as the catalysts [4]. In the gas phase, propane selective oxidation is commonly carried out at temperatures above 573 K with oxygen as the oxidant and supported oxides containing one or several metals (e.g., V, Mo, W, Ni, Co, Nb, Bi) as the catalysts [1,2,10].

In the past decade, gold nanometer-sized supported catalysts have emerged as a novel group of materials because of their high selectivity for several oxidation reactions in both the liquid and gas phases [16–18]. Recent work has shown that in the liquid phase, Au/C effectively catalyzes the epoxidation of *cis*-cyclooctene [19], and Au–Pd/TiO_2 catalyzes the oxidation of alcohols to aldehydes [20]. Other studies in the gas phase have shown that Au supported on transition metal oxides (e.g., TiO_2, Fe_2O_3, Co_2O_3) has high activity for CO oxidation [21,22], and that Au on Ti-containing oxides has high selectivity for propylene epoxidation with H_2 and O_2 [23–25]. Despite efforts toward the development of Au oxidation catalysts, there have been few studies on the selective oxidation of less reac-

* Corresponding author at: Environmental Catalysis and Nanomaterials Laboratory, Department of Chemical Engineering (0211), Virginia Polytechnic Institute and State University, Blacksburg, VA 24061, USA. Fax: +1 540 231 5022.

E-mail address: oyama@vt.edu (S.T. Oyama).

0021-9517/$ – see front matter
doi:10.1016/j.jcat.2008.01.030

tive, more abundant light alkanes, such as methane, ethane, and propane [23,26–28].

Propylene oxide (PO) is a major chemical intermediate with a worldwide estimated production of 6.7 million tons in 2003 [29,30]. Currently, PO is produced mainly from propylene by various multistep, capital-intensive conventional processes. Recently, there has been increasing interest in developing new direct PO synthesis methods to replace inefficient conventional ones, such as the chlorohydrin and organic hydroperoxide processes [31]. Direct processes for the synthesis of PO from propylene typically use O_2 (with $Ag/CaCO_3$ [32–34], Ti/HSZ [35], Ti/SiO_2 [36], and MoO_2/SiO_2 [37] catalysts), H_2O_2 (with titanosilicate catalysts [38,39]), or H_2–O_2 mixtures (with Au/TiO_2 [24,40], $Au/Ti–SiO_2$ [41–45], $Ag/Ti–SiO_2$ [46], and $Pd–Pt/Ti–SiO_2$ [47] catalysts) as the oxidants. The H_2–O_2 route using Au supported on mesoporous $Ti–SiO_2$ (Ti/Si = 3/100) [25,42] and microporous TS-1 (Ti/Si = 1/100) [43–45] has attracted particular attention because of the high selectivity to PO (>90%) and the lower cost of the feedstock compared with expensive H_2O_2. PO space-time yields (STYs) with H_2 and O_2 mixtures at 0.1 MPa and temperatures below 473 K on Au/(mesoporous) $Ti–SiO_2$ and Au/TS-1 are 92 [25,42] and 112 [43–45] $g\,kg_{cat}^{-1}\,h^{-1}$, respectively, with propylene conversions close to 8%, PO selectivities >80%, and H_2 efficiencies >20%, which are close to estimated commercially viable values of >10% C_3H_6 conversion, >90% PO selectivity, and >50% H_2 efficiency [25].

The propylene used to make PO by conventional processes is produced as a byproduct of ethylene manufacture by steam-cracking of higher hydrocarbons or as a byproduct of fluid catalytic cracking units [48]. A one-stage process for the manufacture of PO that can use propane instead of propylene as the feed would have substantial cost advantages. Capital costs could be reduced by as much as 50% by eliminating the need for thermal crackers and associated equipment [49]. Despite this cost advantage, however, little work has been reported on the direct production of PO from propane. One effort in this area is a patent assigned to SRI International claiming that a catalyst composed of $Ag/Cl/NaNO_3/La/Cr/BaCO_3$ converted propane to PO at a propane conversion of 10% and PO selectivity of 8%, resulting in a PO STY of 2.0 $g\,kg_{cat}^{-1}\,h^{-1}$ after 0.3 h at 753 K and 0.1 MPa [50]. But this catalyst deactivated after 5 h of reaction, yielding a propane conversion of about 21%, a PO selectivity of <1%, and a PO STY of about 0.4 $g\,kg_{cat}^{-1}\,h^{-1}$. Another approach to the direct synthesis of PO from propane involves the use of two consecutive reactions: dehydrogenation of propane to propylene and epoxidation of propylene to PO. This process, shown schematically in Fig. 1, is discussed in detail later. Although many catalysts are known to be active for the production of propylene from propane (Fig. 2) [51–70], the direct propane-to-PO process is not possible with current catalysts, because production of propylene (by, e.g., oxidative dehydrogenation) typically occurs at temperatures much higher (>673 K) (Fig. 2) than those required for propylene epoxidation with H_2 and O_2 (<473 K). Consequently, new catalysts able to dehydrogenate propane at temperatures below 473 K are needed to carry out

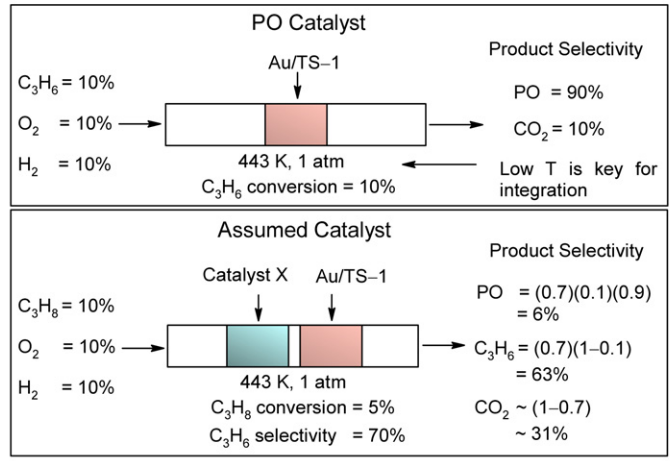

Fig. 1. Hypothetical propane to propylene oxide process.

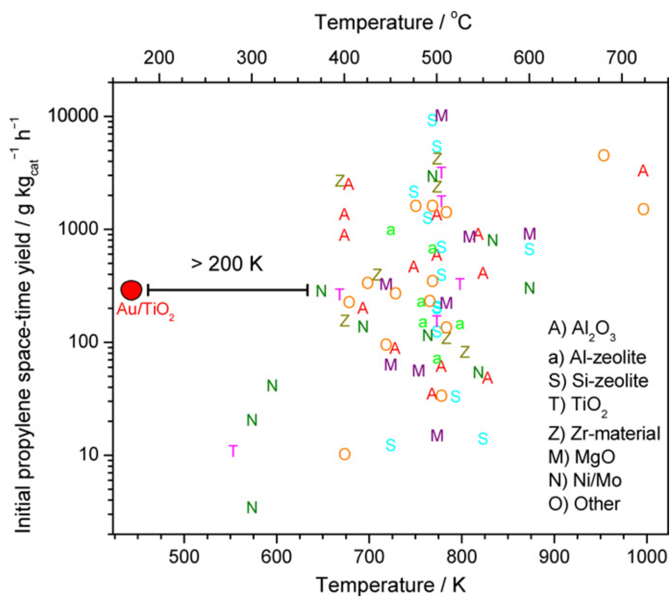

Fig. 2. Review of propylene space-time yields of catalysts for propane oxidative dehydrogenation (arbitrarily classified by major component or support) as a function of temperature. Catalysts include (A) V, Cr, Mo–Al_2O_3 [51–54]; (a) V, Cr, Mg, Co–Al-zeolites (HY, HBEA, USY) [55,56]; (S) V, Cr, Nb–Si-materials (MCM41, MCM48, SiO_2, SBA15, HMS) [57–60]; (T) V, Cr, Sb–TiO_2 [52,53,60]; (Z) V, Cr, Mo–ZrO_2 [52,54,61]; (M) V, Cr, Mo–MgO [62–64]; (N) V, Ni, Mo, Mg, Co, Mn mixed oxides [65–67]; and (O) V, Sb, Mn, Sm, Nb, La, Sr mixed oxides [68–70]; among others [1].

the single-reactor propane dehydrogenation–propylene epoxidation process.

The first part of this work describes a new catalytic system based on Au/TiO_2 that is effective for the transformation of propane to propylene in the presence of H_2 and O_2 gas mixtures (also used for propylene epoxidation on gold catalysts) at low temperatures (<473 K) (Fig. 2). This first part also presents in situ X-ray absorption near-edge structure (XANES) and ultraviolet–visible (UV–vis) spectroscopic characterization of the Au/TiO_2 catalyst under propane dehydrogenation reaction conditions. The spectroscopy results demonstrate activation of oxygen species on gold, which could be involved in the formation of reaction intermediates for the production of propylene. A second part of the work presents the one-step synthesis of PO from propane by sequential propane dehydrogenation on Au/TiO_2 and propylene epoxidation on Au/TS-1 at moderate temperatures (<473 K) and pressures.

2. Experimental

2.1. Catalyst preparation

A mesoporous SiO_2 (Si–TUD) support was synthesized following a method similar to that reported by Jansen et al. [71]. The titanosilicate TS-1 (Ti/Si = 1/100) support was prepared by the method of Khomane et al. [72]. Gold supported catalysts (i.e., Au/TiO_2, Au/TS-1, and Au/Si–TUD) were prepared by the deposition–precipitation (DP) method [73].

The Au/Si–TUD (catalyst 1) was prepared following the method described by Nijhuis et al. [40]. In brief, 5.0 g of Si–TUD was dispersed in 100 ml of H_2O, and the pH was adjusted to 9.5 with 2.5 wt% NH_4OH. A gold solution (105 mg of $HAuCl_3 \cdot 4H_2O$ in 40 ml of water, ∼1 wt% Au/g support) was added dropwise to the support along with the NH_4OH solution to keep the pH at ∼9.5. After stirring for 1 h at ambient conditions, the slurry was filtered and then washed with 0.6 L of water. The resulting solid was vacuum-dried overnight at 298 K, and calcined in air at 673 K (∼3 $K\,min^{-1}$) for 4 h.

For the synthesis of the Au/TS-1 (catalyst 2), 100 ml of a gold solution (3 g of $HAuCl_4 \cdot 4H_2O$ in 1 L of water, 7.2×10^{-3} M) was heated to 343 K under vigorous stirring. The pH of the solution was adjusted to 7.0 by addition of 1 M NaOH (Wako, 97.0+%), followed by the addition of 1.0 g of TS-1. The suspension was stirred for 1 h and then cooled to room temperature. Solids were separated by centrifugation and washed twice with 50 ml of water (Millipore, Autopure WEX 3, Yamato). The solid thus obtained was vacuum-dried overnight at 298 K and was left uncalcined.

In the synthesis of a typical Au/TiO_2 (catalyst 3), 150 ml of a gold solution (1 g of $HAuCl_4 \cdot 4H_2O$, Wako, 99+%, in 1 L of water, 2.4×10^{-3} M) was heated to 343 K under vigorous stirring. The solution pH was brought to 8.8 within 10 min by dropwise addition of 1 M Na_2CO_3 (Wako, 99.5%), followed by addition of 1.5 g of TiO_2 (P25, Nippon Aerosil, 50 $m^2\,g^{-1}$). After 1 h of stirring, the slurry was cooled to room temperature, filtered, and washed with 0.6 L of water (Millipore, Autopure WEX 3, Yamato). The wet solid was vacuum-dried overnight at 298 K and calcined in air at 673 K (∼3 $K\,min^{-1}$) for 3 h. Catalysts 4–7 were prepared by adjusting the gold solution concentration to 3.6×10^{-3}, 4.8×10^{-3}, 7.2×10^{-3}, and 10.1×10^{-3} M, respectively, using a proportional amount of washing water (0.9, 1.2, 1.8, and 2.5 L, respectively).

2.2. Characterization

Transmission electron microscopy (TEM) images of the samples were obtained in a microscope (UT-Philips CM200) operated at 200 kV. In situ Au L_3-edge X-ray adsorption fine-structure (XAFS) measurements were carried out at beamline BL9A of the Photon Factory in the Institute of Materials Structure Science, High-Energy Accelerator Research Organization (PF-IMSS-KEK) in Japan. All spectra were obtained in transmission mode using an in situ XAFS cell under reactions conditions. XAFS data were analyzed with commercially available software (REX, Rigaku Co.). In situ ultraviolet–visible (UV–vis) spectra were collected under the reaction conditions using a large-compartment spectrometer (Varian Cary 5000) equipped with a Harrick Scientific reaction chamber (Model HVC-DRP) and a praying mantis diffuse reflectance attachment (DRP-XXX). Gold content in the samples was estimated from the Au L_3-edge XAFS edge-jump absorption intensity by comparing it with that of a sample of known Au concentration, whereas chlorine content was measured by X-ray fluorescence spectrometry (Rigaku ZSX mini).

2.3. Catalytic testing

Propane partial oxidation was carried out in a quartz tubular microreactor (6 mm diameter, 180 mm long) using powder catalyst samples without dilution (particle size <212 μm, 50 mg for Au/Si–TUD and Au/TiO_2, and 300 mg for Au/TS-1). The empty space before and after the catalyst sample was filled with glass wool to avoid gas-phase reactions. In the case of a two-catalyst bed (Au/TiO_2 and Au/TS-1), catalysts were separated by a thin layer of glass wool. The relative proportion of the Au/TiO_2/Au/TS-1 catalysts by weight was 1/6. Flow rates of C_3H_8 (Takachiho Chemical, purity ⩾99.5%), C_3H_6 (Takachiho Chemical, purity ⩾99.8%), H_2 (from a hydrogen generator, OPGU-2100S, Shimadzu, purity ⩾99.99%), O_2 (Tomoe Shokai, purity ⩾99.5%), and Ar (Suzuki Shokan, purity ⩾99.9997%) were regulated by mass flow controllers. The reactor was equipped with an axial quartz thermocouple well (2 mm outer diameter) that allowed monitoring of the catalyst bed temperature. Reactor temperature was maintained by an electronic controller. Before the reaction, the catalysts were pretreated using two different modes. In mode 1, for calcined catalysts, the temperature was raised from room temperature to 443 K at a rate of 5 $K\,min^{-1}$ under Ar (30 $cm^3\,min^{-1}$) and kept at 443 K for 0.5 h. In mode 2, for uncalcined catalysts, the temperature was raised from room temperature to 443 K at a rate of 0.5 $K\,min^{-1}$ under C_3H_8, H_2, O_2, and Ar. Typical flow rates of reactant gases C_3H_8, H_2, O_2, and Ar were 6, 3, 3, and 18 $cm^3\,min^{-1}$, respectively, with the total pressure set at 0.1 MPa and the temperature controlled at 443 K during the reaction.

Reaction products were analyzed online using two gas chromatographs (Shimazu GC-14), typically after 0.5 h. One of the GCs was equipped with a flame ionization detector (FID) and a thermal conductivity detector (TCD) using a FFAP capillary column (0.32 mm × 60 m) and a Porapak Q packed column (3 mm × 2 m), respectively. The other GC also had one FID and one TCD attached to a Gaskuropak 54 84/100 packed column (3 mm × 2 m) and a MS-5A 60/80 packed column (3 mm × 2 m), respectively. The FFAP capillary column and Porapak Q column were used to detect oxygenates (i.e., acetaldehyde, propylene oxide, acetone, propionaldehyde, acrolein, acetic acid, and 2-propanol), and CO_2 and H_2O, respectively. The Gaskuropak 54 84/100 and MS-5A 60/80 columns were used to detect hydrocarbons (i.e., propane, propylene, ethylene, and ethane), and H_2, O_2, CO, and methane, respectively.

Because the major products observed were propylene (C_3H_6), acetone (CH_3COCH_3), 2-propanol ($CH_3CH(OH)CH_3$), propylene oxide (C_3H_6O), CO_2, and H_2O, the net reactions occurring on the catalysts were taken to be as follows:

$$C_3H_8 + H_2 + O_2 \rightarrow C_3H_6 + 2H_2O,$$

$$C_3H_8 + 2H_2 + 2O_2 \rightarrow CH_3COCH_3 + 3H_2O,$$

$$C_3H_8 + H_2 + O_2 \rightarrow CH_3CH(OH)CH_3 + H_2O,$$

$$C_3H_8 + 2H_2 + 2O_2 \rightarrow C_3H_6O + 2H_2O,$$

$$C_3H_8 + 5O_2 \rightarrow 3CO_2 + 4H_2O,$$

and

$$H_2 + 1/2O_2 \rightarrow H_2O.$$

Based on these reactions, propane conversion, selectivity (to C_3H_6, CH_3COCH_3, $CH_3CH(OH)CH_3$ and C_3H_6O), and H_2 efficiency (selectivity) were defined as follows:

Propane conversion

$$= \text{moles of } (C_3 \text{ products} + CO_2/3)/\text{moles of propane in feed.}$$

C_3 product selectivity

$$= \text{moles of } C_3 \text{ product/moles of } (C_3 \text{ products} + CO_2/3).$$

H_2 efficiency

$$= \text{hydrogen consumed by desired reactions/total hydrogen consumption.}$$

For propane oxidation: on Au/TS-1, H_2 efficiency = $(2 \times$ mol of $CH_3COCH_3 + 1 \times$ mol of $CH_3CH(OH)CH_3)$/total hydrogen consumption; on Au/TiO_2, H_2 efficiency = $(1 \times$ mol of $C_3H_6)$/ total hydrogen consumption; and on the dual Au/TiO_2 + Au/TS-1 catalysts, H_2 efficiency = $(1 \times$ mol of $C_3H_6 + 2 \times$ mol of $C_3H_6O)$/total hydrogen consumption. For propylene epoxidation with H_2 and O_2 ($C_3H_6 + H_2 + O_2 \rightarrow C_3H_6O + H_2O$), similar but simpler equations were used because the main products were PO, CO_2, and H_2O; for example, H_2 efficiency = $(1 \times$ mol of $C_3H_6O)$/(total hydrogen consumption $\approx$ total moles of water) [74].

Turnover frequencies (TOFs) % were calculated based on exposed gold atoms. These were estimated from their particle size assuming truncated octahedral shapes.

The absence of internal mass transfer limitations was checked by means of the Weisz–Prater criterion, $C_{WP} = -r'_{A(obs)}\rho_c R^2/(D_e C_{As}) < 1$, where $-r'_{A(obs)}$ is the observed reaction rate in $kmol\,kg_{cat}^{-1}\,s^{-1}$; ρ_c is the solid catalyst density, in $kg\,m^{-3}$; R is the catalyst particle radius, in m; D_e is the effective gas-phase diffusivity, in $m^2\,s^{-1}$; and C_{As} is the gas concentration of A at the catalyst surface, in $kmol\,m^{-3}$ [75]. For $-r'_{A(obs)} = 2.7 \times 10^{-6}\ kmol\,kg_{cat}^{-1}\,s^{-1}$, $\rho_c = 4000\ kg\,m^{-3}$, $R = 1.06 \times 10^{-4}$ m, estimated propylene $D_e \sim 2.6 \times 10^{-5}\ m^2\,s^{-1}$ [75,76], and $C_{As} \sim 5.6 \times 10^{-3}\ kmol\,m^{-3}$, the C_{WP} is $8 \times 10^{-4} < 1$.

3. Results

Table 1 summarizes the catalytic activities of the gold-supported catalysts for propane partial oxidation. No partial oxidation products were observed when Au/Si–TUD (catalyst 1) was used as the catalyst, for which the only observed product was water due to hydrogen combustion. The main partial oxidation products for Au/TS-1 (catalyst 2) were acetone, 2-propanol, and CO_2, whereas those for Au/TiO_2 (catalyst 3) were propylene, acetone, and CO_2. When using Au/TS-1, selectivities for acetone and 2-propanol were 84 and 10%, respectively, at a propane conversion of 1.1%, resulting in an acetone STY of 26 $g\,kg_{cat}^{-1}\,h^{-1}$ and a TOF of $9.0 \times 10^{-3}\ s^{-1}$ based on exposed gold. In the case of Au/TiO_2, the selectivities to propylene and CO_2 were 69 and 27%, respectively, at a propane conversion of 1.4%, which resulted in a propylene STY of 120 $g\,kg_{cat}^{-1}\,h^{-1}$ and a TOF of 0.029 s^{-1} based on exposed gold. Catalysts presented average particle sizes in the 2.7–4.0 nm range with gold contents of 0.1 wt% for the Au/TS-1 and about 1.0 wt% for the Au/TiO_2 and Au/Si–TUD.

Gold-supported titania catalysts were prepared with average gold particle diameters (D_p) of 2.7–4.1 nm and average Au content of 1.2–2.2 wt%. Fig. 3 presents TEM images and particle size distributions of Au/TiO_2, catalysts 3, 6, and 7, with increasing gold loadings (Table 2). Catalysts 3, 6, and 7 had numerous gold particles with narrow particle size distributions centered at 2.7, 3.1, and 4.1 nm, respectively, in line with their corresponding gold contents of 1.2, 1.9, and 2.2 wt%.

Table 1
Propane oxidation on gold supported catalysts

Catalyst	[Au] (wt%)	D_p (nm)	Conv. (%)	Selectivity (%)				H_2 eff. (%)	Main product	
			C_3H_8	C_3H_6	Acet.	2-Pr.	CO_2		STY ($g\,kg_{cat}^{-1}\,h^{-1}$)	TOF[a] (s^{-1})
Au/Si–TUD (1)	1.0[b]	3.9	0	0	0	0	0	0	0	0
Au/TS-1 (2)	0.10	3.5	1.1	0	84	10	6	14	26	0.009
Au/TiO_2 (3)	1.2	2.7	1.4	69	4	0	27	13	120	0.029

Note. [Au]: Au content by ICP, D_p: Au average particle diameter by TEM, eff.: efficiency, STY: space-time yield, TOF: turnover frequency, Acet.: acetone, 2-Pr.: 2-propanol.

[a] Based on total exposed Au. Au dispersion is calculated from particle size, assuming truncated octahedral particles.

[b] By XRF. Reaction conditions: $C_3H_8/H_2/O_2/Ar = 2/1/1/6$, space velocities of 36,000 (catalysts 1 and 3) and 6000 $cm^3\,h^{-1}\,g_{cat}^{-1}$ (catalyst 2), 443 K, 0.1 MPa.

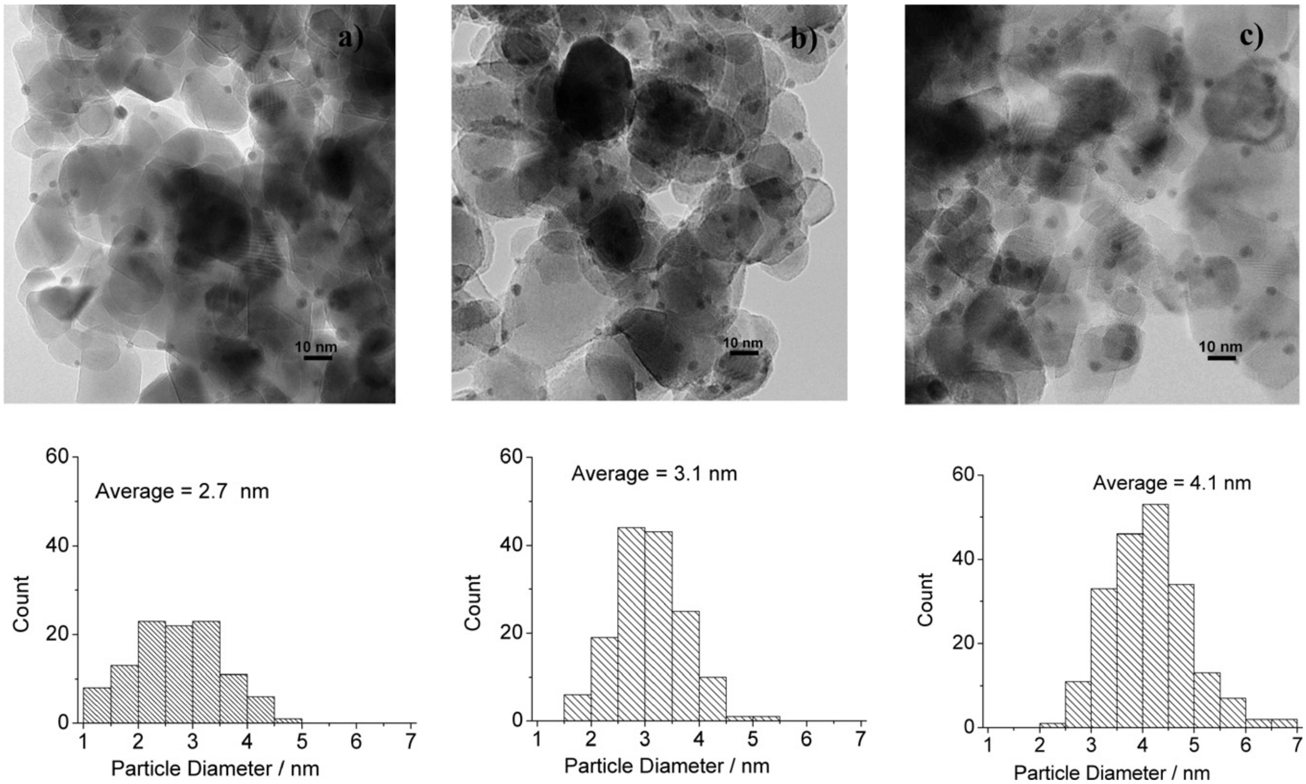

Fig. 3. TEM micrographs and particle size distributions for different Au/TiO_2 catalysts: (a) catalyst 3, 1.2 wt% Au/TiO_2; (b) catalyst 6, 1.9 wt% Au/TiO_2; and (c) catalyst 7, 2.2 wt% Au/TiO_2.

Table 2
Propane oxidative dehydrogenation on Au/TiO_2 (P25) catalysts

Catalyst Au/TiO_2	[Au] (wt%)	D_p (nm)	Conv. (%) C_3H_8	Selectivity (%) C_3H_6	Acet.	CO_2	H_2 eff. (%)	Propylene STY ($g\,kg_{cat}^{-1}\,h^{-1}$)	TOF[a] (s^{-1})
(3)	1.2[b]	2.7	1.4	69	4	27	13	120	0.029
(4)	1.4	N.M.	2.0	73	3	24	11	180	N.M.
(5)	1.7	2.9	2.6	76	2	22	10	250	0.045
(6)	1.9	3.1	2.8	76	1	23	10	270	0.047
(7)	2.2	4.1	1.9	73	3	24	10	170	0.033

Note. [Au]: Au content from Au L_3-edge XAS edge-jump absorption intensity, D_p: Au average particle diameter by TEM, eff.: efficiency, STY: space-time yield, TOF: turnover frequency, Acet.: acetone, 2-Pr.: 2-propanol, N.M.: not measured.

[a] Based on total exposed Au. Au dispersion is calculated from particle size, assuming truncated octahedral particles.

[b] By ICP. Reaction conditions: $C_3H_8/H_2/O_2/Ar = 2/1/1/6$, space velocity = 36,000 $cm^3\,h^{-1}\,g_{cat}^{-1}$, 443 K, 0.1 MPa.

Propane catalytic selective oxidation results on Au/TiO_2 catalysts (i.e., catalysts 3–7) are shown in Table 2. This table shows conversions going through a maximum, first rising from 1.4 to 2.8% and then decreasing to 1.9% as Au concentrations increased from 1.2 to 2.2 wt% (catalysts 3–6). This was accompanied by an initial improvement in propylene selectivities from 69 to 76% (catalysts 3–7) and then a drop to 73% (catalyst 7). Propylene STYs and TOFs based on exposed Au presented similar trends, increasing for catalysts 3–6 and decreasing for catalyst 7 (Fig. 4a). A maximum TOF of $4.2 \times 10^{-2}\ s^{-1}$ was observed for catalyst 6 (1.9 wt% Au/TiO_2, $D_p = 3.1$ nm), which also corresponded to a maximum value of propylene STY of 270 $g\,kg_{cat}^{-1}\,h^{-1}$.

Fig. 4a summarizes the TOF trend for propane partial oxidation on Au/TiO_2 as a function of the gold particle size. TOFs were calculated based on total exposed Au without regard for the type of surface atom. This figure also presents the TOFs for CO oxidation on Au/TiO_2 as a function of gold particle size, which exhibited a similar trend as that for propane partial oxidation, that is, increasing TOF with increasing gold particle size from 2.5 to about 3.0 nm, then decreasing TOF with continued gold particle size increase. Fig. 4b shows the estimated total gold fraction of atoms exposed at corners, edges, and crystal faces in a gold particle consisting of the top slice of a truncated octahedron as a function of particle diameter using the equations given by Janssens et al. [77]. In the studied particle size range of 1.5–5.5 nm, the atom fraction (based on total atoms) changed for Au atoms with different coordination numbers (CNs) (i.e., different positions in the particle). For gold atoms at the corners (CN = 5 or 6), the atom fraction de-

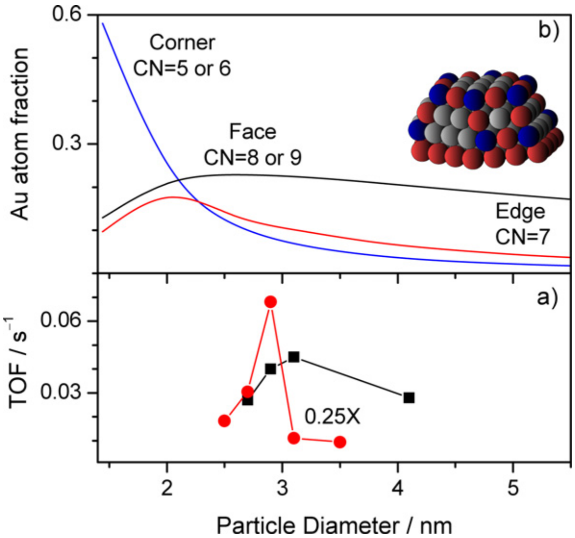

Fig. 4. (a) Turnover frequencies (TOF) as a function of the gold average particle diameter for propane oxidation on Au/TiO_2 at 443 K (squares) and CO oxidation on Au/TiO_2 at 300 K (circles) [22]; and (b) fraction of atoms at corners, edges, and crystal faces in a gold particle consisting of the top slice of a truncated octahedron as a function of particle diameter [77].

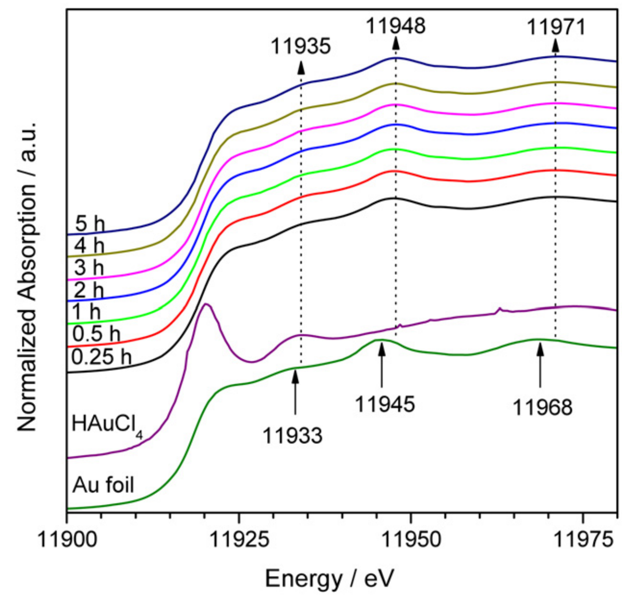

Fig. 6. In situ Au L_3-edge XANES for 1.9 wt% Au/TiO_2 (catalyst 6) under propane selective oxidation conditions as a function of reaction time.

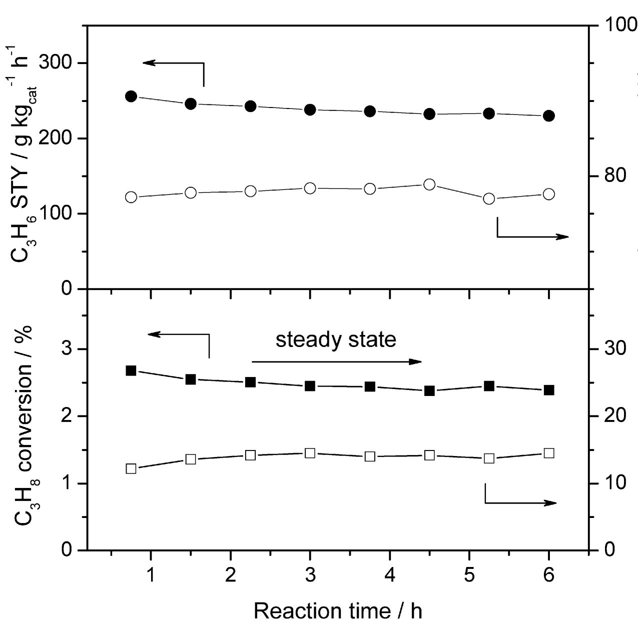

Fig. 5. Propane selective oxidation on 1.9 wt% Au/TiO_2 (catalyst 6) as a function of reaction time.

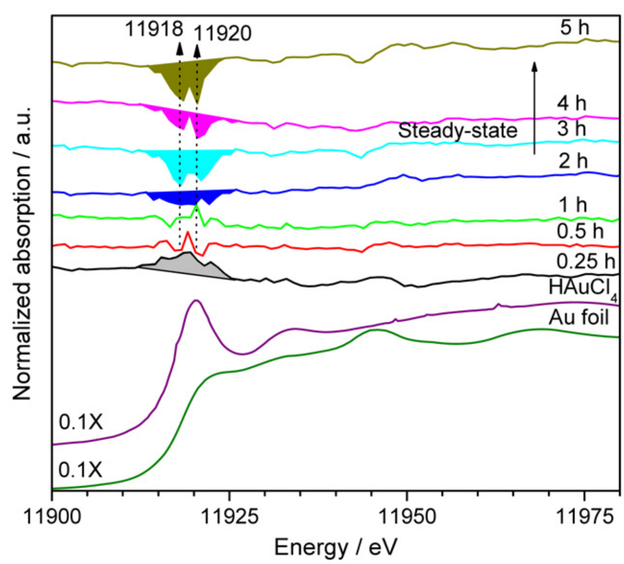

Fig. 7. In situ Au L_3-edge XANES difference spectra, μ(Reaction) − μ(He) at 443 K before reaction, for 1.9 wt% Au/TiO_2 (catalyst 6) at reaction conditions as a function of time on stream.

creased rapidly with increasing particle size, but this decrease slowed after about 3 nm. In the case of gold atoms at the edges (CN = 7), including atoms at the gold–support interface, the atom fraction increased with particle size, reaching a maximum at about 2 nm, after which it gradually decreased. For gold atoms at the faces, the atom fraction also increased with particle size, going from D_p 1.5 to about 2.5 nm, but then decreased slowly with further increases in particle size.

Fig. 5 illustrates the catalytic performance of 1.9 wt% Au/TiO_2 (catalyst 6) for propane partial oxidation with H_2 and O_2 over 6 h. Propane conversion slightly decreased with time but reached a near-steady value of 2.4% after the first 3–4 h. Propylene selectivity remained high and relatively constant (∼80%) during the entire experimental reaction. Hydrogen efficiency also remained relatively constant at 14%. Propylene space-time yield reached a steady value of 235 $g\,kg_{cat}^{-1}\,h^{-1}$.

Fig. 6 shows the in situ Au L_3-edge XANES, normalized to the same edge jump, for the 1.9 wt% Au/TiO_2 (catalyst 6) under reaction conditions as a function of time. The gold foil Au L_3-edge XANES spectrum exhibited three near-edge features at 11,933, 11,945, and 11,968 eV, which are characteristic of Au(0). The in situ Au L_3-edge XANES spectra for 1.9 wt% Au/TiO_2 also showed three peaks at 11,935, 11,948, and 11,971 eV, which also can be attributed to Au(0). The small shift of the features toward higher energies can be attributed to the presence of smaller gold particles in the catalyst [78]. There is no evidence of the presence of cationic gold species, as suggested by the lack of near-edge resonance (white line) at 11,920 eV similar to that observed in a $HAuCl_4$ reference sample. Fig. 7 presents the in situ Au L_3-edge XANES difference spectra μ(Reaction) − μ(He, at 443 K before reaction). The figure demonstrates the evolution of some transient resonance in the initial stages of reaction and the development of two distinct negative features at 11,918 and 11,920 eV after 2–3 h of reaction. They became fully developed at the point at which a steady reaction rate was attained. These features are related to the formation of a Au–O complex by interaction of gold with adsorbed oxygen [79,80], whereas the negative trend indicates that some of the Au–O complex originally present in the air-calcined sample was reduced under reaction conditions.

Fig. 8A presents the UV–vis spectra of Au/TiO_2 (catalysts 3 and 6). The spectra demonstrate bands characteristic of the TiO_2 (P25) support with an additional band centered at about 540 nm (2.3 eV) characteristic of a plasmon resonance of the gold nanoparticles [81–83]. Fig. 8B shows the in situ UV–vis spectra for the 1.9 wt% Au/TiO_2 (catalyst 6) under reaction conditions as a function of time. The spectra exhibited no apparent major changes, with the plasmon resonance position of the gold particles shifting slightly toward lower wavelengths (blue shift) over time. Fig. 9 shows the gold plasmon resonance (PR) position changes during in situ UV–vis measurements under reaction conditions on the 1.9 wt% Au/TiO_2 (catalyst 6). The gold PR position showed an initial transient toward higher wavelengths (red-shift) during the first 0.75 h, followed by a decrease (blue-shift), with an almost constant value (539.3 nm) reached after 2 h of reaction. The initial red-shift of the gold PR position can be assigned to adsorption of oxygen on the gold nanoparticles (Au–O species formation), whereas the blue-shift corresponds to a partial reduction of the Au–O complex by hydrogen or propane present in the reaction gas [84,85]. The PR peak position under H_2/Ar (10 vol%) at 443 K after reaction was 532.9 nm.

Fig. 10 shows the catalytic propane epoxidation with H_2 and O_2 over a two-catalyst bed, 1.9 wt% Au/TiO_2 (catalyst 6, uncalcined) followed by Au/TS-1 (catalyst 2), as a function of time. The catalytic system is relatively stable over the course of the reaction for 12 h, with a propane conversion of 2%, a PO selectivity of 8%, a H_2 efficiency of about 6%, and a PO STY of 4 $g\,kg_{cat}^{-1}\,h^{-1}$.

Table 3 summarizes the results of propane oxidation at steady conditions on 1.9 wt% Au/TiO_2 (catalyst 6, uncalcined), propylene epoxidation on Au/TS-1 (catalyst 2), and propane epoxidation on a sequential two-catalyst bed (catalysts 2 and 6). Propane partial oxidation on uncalcined catalyst 6 presented results similar to those seen for the calcined catalyst 6 one under steady conditions, that is, a slightly higher propane conversion of 2.8%, a slightly lower propylene selectivity of 64%, a lower propane H_2 efficiency of 4%, and a similar propylene STY of 225 $g\,kg_{cat}^{-1}\,h^{-1}$. Propylene epoxidation with H_2 and O_2 on Au/TS-1 (catalyst 2) showed a propylene conversion of 4.7%

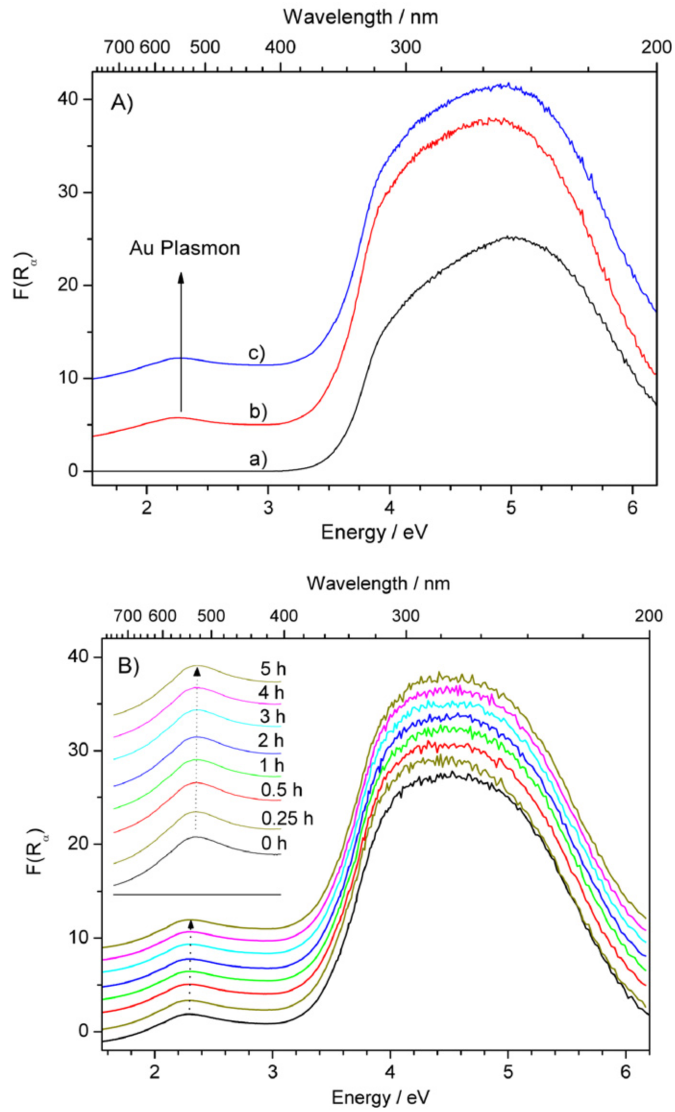

Fig. 8. (A) UV–vis spectra of: (a) TiO_2 (P25) support, (b) 1.2 wt% Au/TiO_2 (catalyst 3), and (c) 1.9 wt% Au/TiO_2 (catalyst 6). (B) In situ UV–vis for 1.9 wt% Au/TiO_2 (catalyst 6) under propane selective oxidation conditions as a function of reaction time. Spectra are referenced to $BaSO_4$.

and a PO selectivity of 89%. H_2 efficiency was 12%. These results yielded a steady PO STY of about 70 $g\,kg_{cat}^{-1}\,h^{-1}$.

4. Discussion

4.1. Hypothetical propane epoxidation process

A hypothetical process for the epoxidation of propane is presented in Fig. 1. This process assumes two consecutive reactions occurring on two different catalysts. In the first reaction, propane is converted to propylene under oxidative conditions with H_2 and O_2 on an oxidative dehydrogenation catalyst (catalyst X), whereas in the second reaction, propylene is transformed to propylene oxide (PO) on a Au/TS-1 catalyst. In this hypothetical system, it is assumed that on catalyst X, propane conversion is 5% at a propylene selectivity of 70%, which is a reasonable guess considering the low reaction temperature and

Table 3
Propane oxidation results at steady-state on a sequential catalyst bed

Catalyst	Gases flow ratio $C_3/H_2/O_2/Ar$	Conv. (%)		Selectivity (%)					H_2 eff. (%)	STY ($g\,kg_{cat}^{-1}\,h^{-1}$)	
		C_3H_8	H_2	PO	C_3H_6	Acet.	2-Pr.	CO_2		C_3H_6	PO
Au/TiO_2 (6)[a]	$2(C_3)/1/1/6$	2.8	95	0	64	2	0	34	4	225	0
Au/TS-1 (2)[b]	$1(C_{3=})/1/1/7$	4.7	30	89	0	3[c]	0	8	12	0	69
Au/TiO_2 (6)[a] + Au/TS-1 (2)[d]	$2(C_3)/1/1/6$	2.0	40	8	57	8	2	25	6	19	4

Note. Eff.: efficiency, STY: space-time yield, C_3: C_3H_8, $C_{3=}$: C_3H_6, PO: propylene oxide, Acet.: acetone, 2-Pr.: 2-propanol, N.M.: not measured, SV: space velocity.

[a] Catalyst (6) left uncalcined, pretreatment mode 2, SV = 36,000 $cm^3\,h^{-1}\,g_{cat}^{-1}$, results after 4 h.

[b] Propylene is used instead of propane, SV = 7000 $cm^3\,h^{-1}\,g_{cat}^{-1}$, results after 12 h.

[c] Also propionaldehyde and acrolein.

[d] SV ~ 5100 $cm^3\,h^{-1}\,g_{cat}^{-1}$, results after 12 h. Relative proportion of Au/TiO_2/Au/TS-1 catalysts weight = 1/6. Reaction conditions: 443 K, 0.1 MPa.

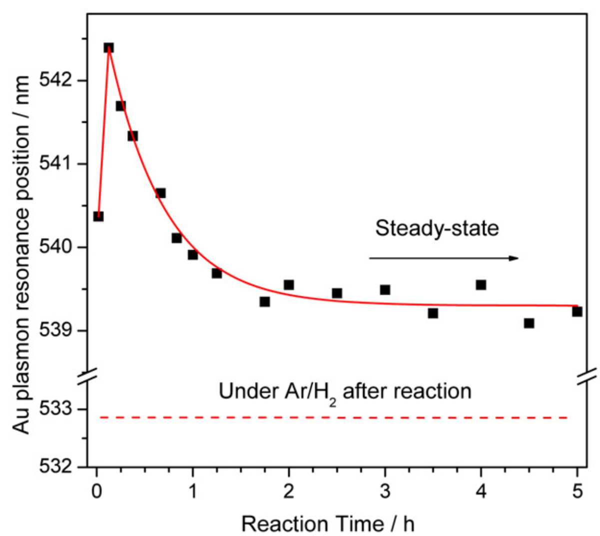

Fig. 9. In situ UV–vis gold plasmon resonance position for 1.9 wt% Au/TiO_2 (catalyst 6) under reaction conditions as a function of reaction time.

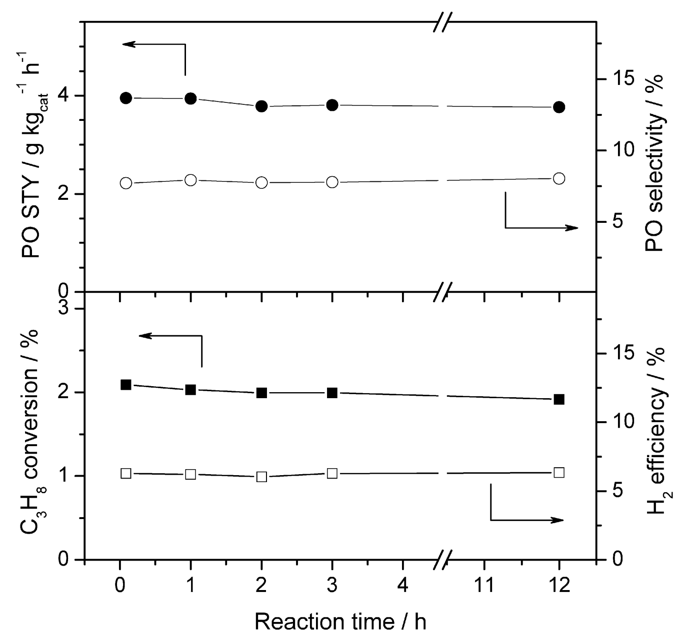

Fig. 10. Propane selective oxidation on a two-catalyst bed, 1.9 wt% Au/TiO_2 (catalyst 6, uncalcined) followed by Au/TS-1 (catalyst 2), as a function of reaction time.

the relatively high propylene selectivity [1]. It is also assumed that on the Au/TS-1 catalyst, the propylene conversion is 10% at a PO selectivity of 90%, which is also a rational estimate based on existing gold-supported catalysts [25,42–45]. CO_2 is a byproduct in both reactions. Using the definition of product selectivity given in the catalyst testing section, it can be shown that the overall product selectivity for the propane epoxidation process is given as follows:

$$\text{Overall PO selectivity} = (C_3H_6\ \text{sel.})_1(C_3H_6\ \text{conv.})_2(\text{PO sel.})_2 = (0.7)(0.1)(0.9) = 6\%;$$

$$\text{Overall } C_3H_6 \text{ selectivity} = (C_3H_6\ \text{sel.})_1(1 - C_3H_6\ \text{conv.})_2 = (0.7)(1 - 0.1) = 63\%;$$

$$\text{Overall } CO_2 \text{ selectivity} = (CO_2\ \text{sel.})_1 + (C_3H_6\ \text{sel.})_1(C_3H_6\ \text{conv.})_2(CO_2\ \text{sel.})_2 = (0.3) + (0.7)(0.1)(0.1) = 31\%.$$

Here the subscript numbers refer to propane dehydrogenation (reaction 1) or propylene epoxidation (reaction 2).

Based on this theoretical exercise, overall PO selectivities in a propane epoxidation process under the aforementioned conditions would be expected to be relatively small, around 6% [50]. In this assumed consecutive dehydrogenation–epoxidation reaction scheme, the overall PO selectivity would be highly influenced by the level of propylene conversion in the epoxidation step because of its relatively small value. Overall PO selectivity should increase with increasing propylene conversion (in reaction 2), whereas overall propylene selectivity should decrease. Moreover, because of the high PO selectivity in the epoxidation step, the overall CO_2 selectivity should be strongly controlled by the CO_2 selectivity in the propane dehydrogenation reaction. Although propane conversion does not appear in the product selectivity, it should affect the overall process yield. From Fig. 1, the adiabatic temperature change ($\Delta T_{adiab.}$) at steady state also could be estimated using $\Delta T_{\text{adiab.}} \approx X[-\Delta H^0_{Rx}]/[\Sigma F_{i0}C_{pi}/F_{A0}]$, where X is conversion, ΔH^0_{Rx} is the standard enthalpy change of reaction, C_{pi} is the mean heat capacity of species i, and F_{i0} and F_{A0} are the molar flow rates of species i and A, respectively [75]. For catalyst X in Fig. 1, propane (species A) conversion was 0.05, ΔH^0_{Rx} was estimated as $-238\ \text{kJ mol}^{-1}$, the average value of the enthalpy of propane dehydrogenation with O_2 ($C_3H_8 + O_2 \rightarrow C_3H_6 + H_2O$; $\Delta H^0_{Rx} = -117\ \text{kJ mol}^{-1}$) and with H_2 and O_2 at 298 K ($C_3H_8 + H_2 + O_2 \rightarrow C_3H_6 + H_2O$; $\Delta H^0_{Rx} = -359\ \text{kJ mol}^{-1}$), and the feed heat capacity, $\Sigma F_{i0}C_{pi}/F_{A0}$, is taken as $0.35\ \text{kJ mol}^{-1}\ \text{K}^{-1}$, resulting in an adiabatic temperature rise of 34 K. In this hypothetical worst-case scenario, when the reaction is carried out adiabatically rather than isothermally as studied here, the reactor temperature still will be relatively moderate and close to 473 K. With current known catalysts, propane oxidative dehydrogenation (ODH) can be achieved directly; however, although the reaction is not limited by equilibrium, it requires high reaction temperatures [60,86]. Examples of catalysts for propane ODH include V, Cr, or Mo supported on Al_2O_3 [51–54], Al-containing zeolites [55,56], SiO_2 [57–60], TiO_2 [52,53,60], ZrO_2 [52,54,61], and MgO [62–64], as well as mixed oxides containing V–Ni–Mo–Mg [65–67] or V–Sb–Mn–Sm [68–70]. Adequate ODH propylene productivities (e.g., space-time yields) have been obtained only at temperatures exceeding about 673 K (Fig. 2) [1,3]. Thus, a key aspect in the integration of the dehydrogenation–epoxidation reactions is the use of moderate temperatures (<473 K) similar to those used in the epoxidation of propylene on gold-supported titanosilicates. Consequently, the development of a catalytic system able to carry out propane dehydrogenation at such moderate temperatures is critical to an integrated propane epoxidation process. We describe such a catalytic system in the next section.

4.2. Propane oxidative dehydrogenation on gold-supported titania

Hydrocarbon-selective oxidation with H_2 and O_2 on gold catalysts was first reported by Haruta et al. [23,24]. Gold-supported titania was shown to catalyze the epoxidation of propylene at low temperatures (<393 K) at high selectivity (>90%), resulting in initial PO space-time yields of about $9\ \text{g kg}^{-1}_{\text{cat}}\ \text{h}^{-1}$ [24]. But the catalyst rapidly deactivated after a couple of hours. Since these first reports, considerable work has been applied toward developing gold supported catalysts, with titanosilicate supports found to be particularly effective for the reaction [25,41–45]. Despite this considerable interest in gold-supported catalysts for hydrocarbon selective oxidation, work on less reactive alkanes, such as propane, is lacking. One short report published more than a decade ago claimed that $Au/TiO_2/SiO_2$ oxidized propane to produce only CO_2 (∼50%) and acetone (∼50%) at rather low yields ($<1\ \text{g kg}^{-1}_{\text{cat}}\ \text{h}^{-1}$) [23]. More recent work on propane oxidation over various gold-supported metal oxides (e.g., CoO_x, MnO_x, CuO, Fe_2O_3, and CeO_2) yielded only CO_2 and H_2O [26–28].

Table 1 presents the results for propane oxidation on gold-supported catalysts with Ti- and Si-containing supports. Gold supported on SiO_2 (Si–TUD, catalyst 1) was not active for propane oxidation, and the only reaction product was H_2O from hydrogen combustion. This is in agreement with the results of Barton and Podkolzin [87], who studied H_2O formation from H_2 and O_2 on gold nanoparticles supported on SiO_2. Gold supported on TS-1 (Ti/Si = 1/100, catalyst 2) oxidized propane to produce oxygenated products, acetone, and 2-propanol, with combined selectivities of >90% at a propane conversion of about 1%. The STY of acetone was $26\ \text{g kg}^{-1}_{\text{cat}}\ \text{h}^{-1}$, much greater than the previously reported value of $1\ \text{g kg}^{-1}_{\text{cat}}\ \text{h}^{-1}$ [23]. The TOF of acetone based on exposed Au was $9.0 \times 10^{-3}\ \text{s}^{-1}$, which is in the same order of magnitude as the PO TOFs reported for Au–Ba/Ti–TUD catalysts [74]. But gold supported on titania (1.2 wt% Au/TiO_2, catalyst 3) oxidized propane to produce mostly propylene with high selectivity (∼70%), CO_2 (∼25%), and acetone (∼5%) at a propane conversion of 1.2%. This latter result is quite unique, because propane was oxidatively dehydrogenated at a quite moderate temperature of 443 K. The STY of propylene on 1.2 wt% Au/TiO_2 (catalyst 3) was $120\ \text{g kg}^{-1}_{\text{cat}}\ \text{h}^{-1}$, which compares well with the typical STYs for propane ODH catalysts, even though they operate at much higher reaction temperatures (Fig. 2). The TOF of propylene TOF based on exposed Au ($0.029\ \text{s}^{-1}$) also had the same order of magnitude as the TOFs observed for propylene epoxidation on gold-supported titanosilicates [74]. These results confirm the need for both Au nanosized particles and Ti in catalysts active for hydrocarbon-selective oxidation [24], because neither support alone nor gold on silica was active for propane partial oxidation.

A series of gold-supported titania catalysts with varying gold content were prepared using the DP synthesis method (Table 2). The gold content in the catalysts varied from 1.2 to 2.2 wt%, with average gold particle diameters (D_p) increasing from 2.7 to 4.1 nm (catalysts 3–7). Typical TEM images for 1.2 wt% Au/TiO_2 (catalyst 3), 1.9 wt% Au/TiO_2 (catalyst 6), and 2.2 wt% Au/TiO_2 (catalyst 7) are shown in Fig. 3. The catalysts had numerous gold particles with a narrow size distribution, as expected for catalysts prepared by the DP method. Propane oxidation results on Au/TiO_2 catalysts demonstrated increased propylene STY in going from catalyst 3 to 6, then decreasing for catalyst 7. An optimum propylene STY of $270\ \text{g kg}^{-1}_{\text{cat}}\ \text{h}^{-1}$ was obtained for 1.9 wt% Au/TiO_2 (catalyst 6), which had an intermediate gold content (1.9 wt%) and average particle size (3.1 nm) and exhibited the highest propane conversion (2.8%) and propylene selectivity (76%) among the catalysts studied. TOFs of propylene based on exposed gold also showed a similar trend as that for propylene STY, that is, TOFs reaching a maximum for catalysts 3 to 6 and then decreasing for catalyst 7. This trend in TOFs indicates a particle size effect (Fig. 4a). These results are reminiscent of the gold particle size dependency on Au/TiO_2 catalysts in CO oxidation [22,88], which was greatest at a D_p of 2.9 nm (Fig. 4a). In that case, the particle size dependency was ascribed to a contribution from the perimeter interface between Au particles and the TiO_2 support [22], as well as a quantum size effect related to the thickness of the Au particles [88]. The gold particle size dependency in propane oxidation is likely to arise from an optimum population of highly uncoordinated Au atoms on small particles (Fig. 4b), which could contribute to the stabilization of reaction intermediates involving H_2 and O_2 [89–92]. Recently, the catalytic oxidation of hydrogen over Au/TiO_2 catalysts was studied in the presence of propane at temperatures between 298 and 873 K. In that study, the only propane oxidation products reported were CO and CO_2. This is in contrast with the results of the present work demonstrating production of propylene. This lack of propylene formation may be related to the different methods of catalyst preparation, the smaller size of the gold nanoparticles (1.1–1.4 nm), and the different gas ratios ($C_3H_8/H_2/O_2/H_2 = 10/2/0.5–2/86–87.5$) [93].

Propane partial oxidation on 1.9 wt% Au/TiO_2 (catalyst 6) as a function of time demonstrated that the catalyst was relatively stable, with little deactivation observed over a 6-h period (Fig. 5). After a slight drop, the conversion stabilized after about 3–4 h of reaction, resulting in a propylene STY of 235 $g\,kg_{cat}^{-1}\,h^{-1}$. These results were contrary to what was observed for propylene epoxidation with H_2 and O_2 over Au/TiO_2 catalysts, which deactivated quite rapidly after 1–2 h of reaction [24,31,40]. This deactivation was related to the decomposition of PO on Ti acidic sites [94]. The stability of the Au/TiO_2 catalyst during propane oxidation was likely related to the fact that the propylene product desorbed and did not decompose and deposit on the Ti active sites.

The in situ Au L_3-edge XANES results for 1.9 wt% Au/TiO_2 (catalyst 6) show that the catalyst contained mostly Au(0) (Fig. 6). The presence of oxidized gold components, as evidenced by a near-edge resonance around 11,920 eV (e.g., $HAuCl_4$), was not detected for this catalyst during the in situ measurements under propane partial oxidation conditions. The intensity of the first feature in the Au L_3-edge (white line) arises from unoccupied d-states, and thus interactions between adsorbed molecules and gold clusters should reflect changes in this resonance [79,80]. The in situ Au L_3-edge XANES difference spectra $\mu(\text{Reaction}) - \mu(\text{He, at 443 K before reaction})$ (Fig. 7) reveal the evolution of a transient resonance (white line) during the first 1.5 h of reaction, followed by the full development of two negative features at 11,918 and 11,920 eV after 2–3 h of reaction. The initial increase in intensity of the white line may be related to the chemisorption of oxygen on gold particles (Au–O complex formation), as the d-orbital electron count of gold decreases due to charge transfer to the $2\pi^*$ orbital of oxygen [79,80]. The further decrease and formation of negative features as the reaction reached a steady value after 2–3 h, corresponds to a reduction of the Au–O complex (in the air-calcined sample) by reaction with H_2. Similar trends have been reported for a 4 wt% Au/Al_2O_3 catalyst subsequently exposed to O_2 and CO—that is, an increase in the intensity of the white line during O_2 exposure, followed by a decrease in intensity by reaction of the thus-formed Au–O complex with CO to form CO_2 [80].

UV–vis spectra of Au/TiO_2 catalysts (Fig. 8) present two sets of characteristic features, the first due to the TiO_2 support and the second due to the plasmon resonance (PR) of gold nanoparticles. The band due to the TiO_2 was due to d–d transitions and was invariant. The gold plasmon resonance feature was symmetric and centered around 2.28 eV (540 nm), indicating that the gold particles were of regular shape with a narrow size distribution. This is in agreement with TEM results (Fig. 3) showing narrow gold particle size distributions. Measurements of the PR position during in situ UV–vis under propane oxidation on the 1.9 wt% Au/TiO_2 (catalyst 6) (Fig. 9) were used to study the adsorptive properties of the Au nanoparticles. The gold PR position showed an initial (first 0.75 h) shift toward higher wavelengths (red-shift), followed by a shift toward lower wavelengths (blue-shift), with an almost constant value reached after 2–3 h of reaction. The initial red-shift of the PR position was related to the adsorption of O_2 on the gold particles (formation of Au–O species). The red-shift of the resonance can be explained by the lower density of free electrons in the gold as a result of charge transfer from the surface metal atoms to adsorbed O_2 [84,85]. The blue-shift likely resulted from depletion of Au–O species by reaction with H_2 as the reaction reached a steady condition. These findings are consistent with the in situ XANES measurements indicating formation of Au–O species and partial reduction of the oxidized gold. The gold PR position (539.3 nm) at steady rate conditions was higher than that observed for the catalyst under H_2 flow (532.9 nm); this finding suggests the presence of adsorbed O_2 and possibly H_2 on Au during the reaction, which can then react to produce hydroperoxide species [95,96] as a steady rate is reached after 2 h. At present, the nature of the Au–O adsorbed species is unknown. These species could well be any of those previously proposed for Au-supported materials, such as O^-, O^{2-}, or hydroperoxo species [95–97] adsorbed on Au [79,80,98] or at the Au–Ti interface [99].

Additional catalytic experiments were carried out to study the possible presence of hydroperoxide species under propane dehydrogenation conditions using three different gas mixtures: $C_3H_8/O_2/Ar = 2/1/7$ (absence of H_2), $C_3H_8/H_2/Ar = 2/1/7$ (absence of O_2), and $C_3H_8/Ar = 2/8$ (absence of H_2 and O_2). No propylene was produced with the $C_3H_8/O_2/Ar$ and C_3H_8/Ar gas mixtures; however, traces of propylene were observed with the $C_3H_8/H_2/Ar$ gas mixture. In this case, H_2 likely reacted with O_2 adsorbed on Au present in the air-calcined Au/TiO_2 catalyst, as indicated by the high initial Au PR position compared with the Au PR position for the reduced catalyst (Fig. 9). These results suggest the possible involvement of hydroperoxide species in the dehydrogenation of propane, because both H_2 and O_2 are needed for the reaction to take place.

4.3. Propane epoxidation on a two-catalyst bed reactor

Propylene epoxidation catalytic activity on Au/TS-1 (catalyst 2) is characterized by propylene conversions of about 5%, PO selectivities >80%, and remarkable stability with time on stream [44,45]. One-stage propane epoxidation by a consecutive two-bed catalyst composed of 1.9 wt% Au/TiO_2 (catalyst 6) and Au/TS-1 (catalyst 2) resulted in propane conversions of 2% and overall selectivities for PO of 8% (Fig. 10). This PO selectivity value is in agreement with expected values for the hypothetical sequential dehydrogenation–epoxidation process discussed in Section 4.1 (Fig. 1). The PO STY based on total weight of catalysts was 4 $g\,kg_{cat}^{-1}\,h^{-1}$, higher than that reported for a propane epoxidation process using a Ag/Cl/$NaNO_3$/La/Cr/$BaCO_3$ catalyst ($2.0\ g\,kg_{cat}^{-1}\,h^{-1}$) [50]. It is noteworthy that in that work, not only was the reaction temperature 553 K, but also the catalyst deactivated after 5 h, resulting in a PO STY of only $0.4\ g\,kg_{cat}^{-1}\,h^{-1}$. This is a marked difference from the sequential dehydrogenation–epoxidation system presented here, which used a much lower temperature (443 K) and displayed little deactivation over a period of 12 h (Fig. 10). This lack of deactivation was due to the individual Au/TiO_2 and Au/TS-1 catalyst stabilities as presented in Figs. 5 and 10. The use of uncalcined catalyst 6 in the two-catalyst bed reactor would not be expected to influence the process, because its catalytic properties (i.e., propane conversion, propylene selectivity, and STY) are very similar to those of the calcined catalyst (Tables 2 and 3). The PO STY from propane epoxidation ($4\ g\,kg_{cat}^{-1}\,h^{-1}$) is also comparable to earlier findings on propylene epoxidation using similar catalytic systems; for example, Hayashi et al. obtained an initial PO STY of about $10\ g\,kg_{cat}^{-1}\,h^{-1}$ on a deactivating Au/TiO_2 [24], Zwijnenburg et al. reported a PO STY of $10\ g\,kg_{cat}^{-1}\,h^{-1}$ on Au–Pt/TiO_2/SiO_2 [100], de Oliveira et al. reported a PO STY of $4\ g\,kg_{cat}^{-1}\,h^{-1}$ on Ag/TiO_2 [101], and Wang et al. obtained a PO STY of $7\ g\,kg_{cat}^{-1}\,h^{-1}$ on Ag/TS-1 [46]. Considering the similarities between PO STYs of these propylene epoxidation catalysts and the propane epoxidation process of the present study, further advances in the system would be expected to produce better catalytic performance. Two direct changes that could affect the system productivity (STY) would involve improvements in both propane epoxidation steps, that is, propane dehydrogenation (reaction 1) and propylene epoxidation (reaction 2) steps. These improvements should be aimed at increasing propane and propylene conversions in reactions 1 and 2, respectively, while keeping the corresponding propylene and PO selectivities high. As described in Section 4.1, these changes should result in higher overall PO selectivities and thus greater PO STYs; this may be possible by modifying the catalytic system or making appropriate changes to the reactor configuration, for example, using a hydrogen-selective membrane reactor allowing safer use of a wider range of H_2 compositions [102].

There exist theoretical and experimental data regarding the possible sequence of steps occurring during propylene epoxidation with H_2 and O_2 on gold-supported titanosilicate catalysts [103–107]. These steps can be summarized as follows: (1) synthesis of H_2O_2 from H_2 and O_2 on Au [103]; (2) formation of Ti-hydroperoxo or peroxo species from H_2O_2 and tetrahedral Ti centers [96,105–107]; (3) formation of PO from reaction of C_3H_6 with Ti-hydroperoxide species [104]; and (4) decomposition of H_2O_2 to H_2O [87]. Despite this knowledge, however, not as much theoretical or experimental work has been done for selective oxidation on Au/TiO_2 catalysts. Here we speculate that propane dehydrogenation with H_2 and O_2 on Au/TiO_2 may occur through the following simplified steps: (1) synthesis of H_2O_2 from H_2 and O_2 on Au [103]; (2) formation of a 2-propoxy intermediate species from reaction of C_3H_8 on TiO_2 and peroxo or hydroperoxo species from Au [6,7]; (3) formation of C_3H_6 from dehydration of 2-propoxy species [108]; and (4) decomposition of H_2O_2 to H_2O [87]. It has been suggested that H_2O_2 forms from H_2 and O_2 on gold [103]; our in situ XANES (Fig. 7) and UV–vis (Fig. 9) spectroscopic results showing the formation of a Au–O complex and its later reduction suggest that this indeed may be the case on Au/TiO_2 during the dehydrogenation of propane. The main products of reaction of propane oxidation with H_2O_2 in liquid phase are acetone and 2-propanol, due to oxidative attack on the more reactive secondary C–H bond of propane [4,5,8,9]. Likewise, propane oxidation with H_2 and O_2 in the gas phase can occur through a similar oxygenated intermediate (a 2-propoxy species), as suggested by the production of acetone and 2-propanol on Au/TS-1 (Table 1; catalyst 2) and of propylene and acetone as a side product on Au/TiO_2 (Table 1; catalyst 3) [109,110]. This 2-propoxy species could be oxidized to form acetone (on Au/TS-1) or dehydrated to produce propylene (on Au/TiO_2) [108,110]. The reaction pathway described above is significantly different than that proposed for propane ODH with O_2; for example, on typical VO_x catalysts, the reaction has been shown to occur through a Mars–van Krevelen redox mechanism in which lattice oxygen atoms abstract hydrogen from C_3H_8 in an irreversible C–H bond activation step [111].

5. Conclusion

This work demonstrates direct propane epoxidation through sequential propane dehydrogenation–propylene epoxidation on gold catalysts. This single-reactor process was made possible by the finding that Au/TiO_2 is effective for the low-temperature dehydrogenation of propane. A 1.9 wt% Au/TiO_2 catalyst with an average gold particle size of 3.1 nm prepared by the deposition–precipitation method dehydrogenated propane at 443 K and 0.1 MPa in the presence of H_2 and O_2 at a maximum propylene STY of $270\ g\,kg_{cat}^{-1}\,h^{-1}$. In situ XANES and UV–vis spectroscopic characterization of the Au/TiO_2 catalyst under propane reaction conditions showed the formation of a Au–O complex that may react with H_2 to form hydroperoxide species. Production of acetone and 2-propanol on Au/TS-1, and of propylene and acetone on Au/TiO_2, suggests the possible presence of a 2-propoxy intermediate during propane oxidation with H_2 and O_2. The 1.9 wt% Au/TiO_2 catalyst was relatively stable and showed little deactivation after 6 h. The combination in a single reactor of a sequential two-catalyst bed composed of 1.9 wt% Au/TiO_2 followed by a relatively active and stable Au/TS-1 for propylene epoxidation resulted in the direct synthesis of propylene oxide from propane with H_2 and O_2 at 443 K and 0.1 MPa. This process had a propane conversion of 2% and overall PO and propylene selectivities of 8 and 57%, respectively, resulting in a constant STY for PO of $4\ g\,kg_{cat}^{-1}\,h^{-1}$ for at least 12 h. Further improvements in the catalysts and reactor design leading to higher propane and propylene conversions should have a significant affect on the productivity of this process.

Acknowledgments

Financial support was provided by the Ministry of Economy, Trade and Industry (METI, Minimum energy chemistry project) and the National Science Foundation (CBET 0651238). J.J. B.-S. and S.T.O. acknowledge financial support from the Japan Society for the Promotion of Science (JSPS) through the post-doctoral fellowship for foreign researcher program (P05627) and the invited fellow program. The authors also thank Drs. T. Arai and K. Sayama (ETRI, AIST) for assistance with the XRF measurements and Ms. E. Kobayashi and Dr. K. Kawasaki for the TEM measurements. The XAFS experiments were conducted under the approval of PF-PAC (proposals 2004G304 and 2006G362).

References

[1] F. Cavani, F. Trifirò, Catal. Today 24 (1995) 307.
[2] E.A. Mamedov, V. Cortés Corberán, Appl. Catal. A 127 (1995) 1.
[3] F. Cavani, N. Ballarini, A. Cericola, Catal. Today 127 (2007) 113.
[4] P.E. Ellis Jr., J.E. Lyons, J. Chem. Soc. Chem. Commun. (1989) 1315.
[5] N. Mizuno, Catal. Surv. Jpn. 4 (2000) 149.
[6] H. Sun, F. Blatter, H. Frei, Catal. Lett. 44 (1997) 247.
[7] J. Xu, B.L. Mojet, J.G. Van Ommen, L. Lefferts, J. Phys. Chem. B 108 (2004) 218.
[8] M.G. Clerici, Appl. Catal. 68 (1991) 249.
[9] R. Raja, C.R. Jacob, P. Ratnasamy, Catal. Today 49 (1999) 171.
[10] R.K. Grasselli, Catal. Today 49 (1999) 141.
[11] M.M. Lin, Appl. Catal. A 207 (2001) 1.
[12] M.M. Bettahar, G. Costentin, L. Savary, J.C. Lavalley, Appl. Catal. A 145 (1996) 1.
[13] J.C. Vedrine, E.K. Novakova, E.G. Derouane, Catal. Today 81 (2003) 247.
[14] M. Baerns, O.V. Buyevskaya, M. Kubik, G. Maiti, O. Ovsitser, O. Seel, Catal. Today 33 (1997) 85.
[15] S.H. Taylor, G.J. Hutchings, M.L. Palacios, D.F. Lee, Catal. Today 81 (2003) 171.
[16] M. Haruta, Catal. Today 36 (1997) 153.
[17] M. Haruta, Cattech 6 (2002) 102.
[18] A.S.K. Hashmi, G.J. Hutchings, Angew. Chem. Int. Ed. 45 (2006) 7896.
[19] M.D. Hughes, Y.-J. Xu, P. Jenkins, P. McMorn, P. Landon, D.I. Enache, A.F. Carley, G.A. Attard, G.J. Hutchings, F. King, E.H. Stitt, P. Johnston, K. Griffin, C.J. Kiely, Nature 437 (2005) 1132.
[20] D.I. Enache, J.K. Edwards, P. Landon, B. Solsona-Espriu, A.F. Carley, A.A. Herzing, M. Watanabe, C.J. Kiely, D.W. Knight, G.J. Hutchings, Science 311 (2006) 362.
[21] M. Haruta, N. Yamada, T. Kobayashi, S. Iijima, J. Catal. 115 (1989) 301.
[22] G.R. Bamwenda, S. Tsubota, T. Nakamura, M. Haruta, Catal. Lett. 44 (1997) 83.
[23] T. Hayashi, K. Tanaka, M. Haruta, Prep. Am. Chem. Soc. Div. Pet. Chem. 41 (1996) 71.
[24] T. Hayashi, K. Tanaka, M. Haruta, J. Catal. 178 (1998) 566.
[25] B. Chowdhury, J.J. Bravo-Suárez, M. Daté, S. Tsubota, M. Haruta, Angew. Chem. Int. Ed. 45 (2006) 412.
[26] K. Ruth, M. Hayes, R. Burch, S. Tsubota, M. Haruta, Appl. Catal. B 24 (2000) L133.
[27] B.E. Solsona, T. García, C. Jones, S.H. Taylor, A.F. Carley, G.J. Hutchings, Appl. Catal. A 312 (2006) 67.
[28] A.C. Gluhoi, N. Bogdanchikova, B.E. Nieuwenhuys, Catal. Today 113 (2006) 178.
[29] M. Ishino, J. Yamamoto, Shokubai (Catalysts & Catalysis) 48 (2006) 511.
[30] D.L. Trent, Propylene Oxide, Kirk Othmer Encyclopedia of Chemical Technology [Online]; Wiley & Sons, posted June 4, 2001. doi:10.1002/0471238961.1618151620180514.a01.pub2.
[31] T.A. Nijhuis, M. Makkee, J.A. Moulijn, B.M. Beckhuysen, Ind. Eng. Chem. Res. 45 (2006) 3447.
[32] S.T. Oyama, K. Murata, M. Haruta, Shokubai (Catalysts & Catalysis) 46 (2004) 13.
[33] J.Q. Lu, J.J. Bravo-Suárez, M. Haruta, S.T. Oyama, Appl. Catal. A 302 (2006) 283.
[34] J.Q. Lu, J.J. Bravo-Suárez, A. Takahashi, M. Haruta, S.T. Oyama, J. Catal. 232 (2005) 85.
[35] K. Murata, Y. Kiyozumi, Chem. Commun. (2001) 1356.
[36] N. Mimura, S. Tsubota, K. Murata, K.K. Bando, J.J. Bravo-Suárez, M. Haruta, S.T. Oyama, Catal. Lett. 1–2 (2006) 47.
[37] Z.X. Song, N. Mimura, J.J. Bravo-Suárez, T. Akita, S. Tsubota, S.T. Oyama, Appl. Catal. A 316 (2007) 142.
[38] M.G. Clerici, G. Bellussi, U. Romano, J. Catal. 129 (1991) 159.
[39] M.G. Clerici, P. Ingallina, J. Catal. 14 (1993) 71.
[40] T.A. Nijhuis, T. Visser, B.M. Weckhuysen, J. Phys. Chem. B 109 (2005) 19309.
[41] B.S. Uphade, S. Tsubota, T. Hayashi, M. Haruta, Chem. Lett. (1998) 1277.
[42] A.K. Sinha, S. Seelan, M. Okumura, T. Akita, S. Tsubota, M. Haruta, J. Phys. Chem. B 109 (2005) 3956.
[43] T.A. Nijhuis, B.J. Huizinga, M. Makkee, J.A. Moulijn, Ind. Eng. Chem. Res. 38 (1999) 884.
[44] N. Yap, R.P. Andres, W.N. Delgass, J. Catal. 226 (2004) 156.
[45] B. Taylor, J. Lauterbach, W.N. Delgass, Appl. Catal. A 291 (2005) 188.
[46] R. Wang, X. Guo, X. Wang, J. Hao, G. Li, J. Xiu, Appl. Catal. A 261 (2004) 7.
[47] R. Meiers, U. Dingerdissen, W.F. Hölderich, J. Catal. 176 (1998) 376.
[48] A.H. Tullo, Chem. Eng. News 85 (17) (2007) 27.
[49] M.M. Bhasin, S.W. King, US Patent 6,765,101 B1, July 20, 2004, assigned to Union Carbide Chemicals & Plastics Technology Corporation.
[50] G. Mul, M.F. Asaro, A.S. Hirschon, R.B. Wilson Jr., US Patent 6,509,485 B2, January 21, 2003, assigned to SRI International.
[51] S. Yang, E. Iglesia, A.T. Bell, J. Phys. Chem. B 109 (2005) 8987.
[52] F. Arena, F. Frusteri, A. Parmaliana, Catal. Lett. 60 (1999) 59.
[53] M. Cherian, M.S. Rao, A.M. Hirt, I.E. Wachs, G. Deo, J. Catal. 211 (2002) 482.
[54] K.L. Fujdala, T.D. Tilley, J. Catal. 218 (2003) 123.
[55] A. Kubacka, E. Włoch, B. Sulikowski, R.X. Valenzuela, V. Cortés Corberán, Catal. Today 61 (2000) 343.
[56] R. Bulánek, K. Novoveská, B. Wichterlová, Appl. Catal. A 235 (2002) 181.
[57] O.V. Buyevskaya, A. Brückner, E.V. Kondratenko, D. Wolf, M. Baerns, Catal. Today 67 (2001) 369.
[58] J. Santamaría-González, J. Mérida-Robles, M. Alcántara-Rodríguez, P. Maireles-Torres, E. Rodríguez-Castellón, A. Jiménez-López, Catal. Lett. 64 (2000) 209.
[59] R. Zhou, Y. Cao, S. Yan, J. Deng, Y. Liao, B. Hong, Catal. Lett. 75 (2001) 107.
[60] W. Schuster, J.P.M. Niederer, W.F. Hoelderich, Appl. Catal. A 209 (2001) 131.
[61] R. Rulkens, T.D. Tilley, J. Am. Chem. Soc. 120 (1998) 9959.
[62] K. Bahranowski, G. Bueno, V. Cortés Corberán, F. Kooli, E.M. Serwicka, R.X. Valenzuela, K. Wcisło, Appl. Catal. A 185 (1999) 65.
[63] Z.-S. Chao, E. Ruckenstein, Catal. Lett. 94 (2004) 217.
[64] C. Pak, A.T. Bell, T.D. Tilley, J. Catal. 206 (2002) 49.
[65] N. Dimitratos, J.C. Védrine, Catal. Today 81 (2003) 561.
[66] S.N. Koc, G. Gurdag, S. Geissler, M. Muhler, Ind. Eng. Chem. Res. 43 (2004) 2376.
[67] E.V. Kondratenko, O.V. Buyevskaya, M. Baerns, Top. Catal. 15 (2001) 175.
[68] M. Cherian, M.S. Rao, G. Deo, Catal. Today 78 (2003) 397.
[69] L. Yuan, S. Bhatt, G. Beaucage, V.V. Guliants, S. Mamedov, R.S. Soman, J. Phys. Chem. B 109 (2005) 23250.
[70] Z.M. Fang, J. Zou, W.Z. Weng, H.L. Wan, Stud. Surf. Sci. Catal. (Natural Gas Conversion V) 119 (1998) 629.
[71] J.C. Jansen, Z. Shan, L. Marchese, W. Zhou, N.v.d. Puil, Th. Maschmeyer, Chem. Commun. (2001) 713.
[72] R.B. Khomane, B.D. Kulkarni, A. Paraskar, S.R. Swainkar, Mater. Chem. Phys. 76 (2002) 99.

[73] S. Tsubota, D.A.H. Cunningham, Y. Bando, M. Haruta, Stud. Surf. Sci. Catal. (Preparation of Catalysts VI) 91 (1995) 227.
[74] J.Q. Lu, X. Zhang, J.J. Bravo-Suárez, K.K. Bando, T. Fujitani, S.T. Oyama, J. Catal. 250 (2007) 350.
[75] H.S. Fogler, Elements of Chemical Reaction Engineering, third ed., Prentice–Hall PTR, Upper Saddle River, NJ, 2006.
[76] P.E. Liley, G.H. Thomson, D.G. Friend, T.E. Daubert, in: R.H. Perry, D.W. Green (Eds.), Chemical Engineering's Handbook, seventh ed., McGraw–Hill, 1999, Chapter 2.
[77] A. Carlsson, A. Puig-Molina, T.V.W. Janssens, J. Phys. Chem. B 110 (2006) 5286.
[78] R.E. Benfield, D. Grandjean, M. Kröll, R. Pugin, T. Sawitowski, G. Schmid, J. Phys. Chem. B 105 (2001) 1961.
[79] N. Weiher, A.M. Beesley, N. Tsapatsaris, L. Delannoy, C. Louis, J.A. Van Bokhoven, S.L.M. Schroeder, J. Am. Chem. Soc. 129 (2007) 2240.
[80] J.A. Van Bokhoven, C. Louis, J.T. Miller, M. Tromp, O.V. Safonova, P. Glatzel, Angew. Chem. Int. Ed. 45 (2005) 4651.
[81] U. Kreibig, M. Vollmer, Optical Properties of Metal Clusters, Springer, Berlin, 1995.
[82] U. Kreibig, L. Genzel, Surf. Sci. 156 (1985) 678.
[83] L.M. Liz-Marzán, Langmuir 22 (2006) 32.
[84] W. Cai, H. Hofmeister, T. Rainer, Physica E 11 (2001) 339.
[85] W. Cai, H. Hofmeister, T. Rainer, W. Chen, J. Nanopart. Res. 3 (2001) 443.
[86] M.M. Bhasin, J.H. McCain, B.V. Vora, T. Imai, P.R. Pujadó, Appl. Catal. A 221 (2001) 397.
[87] D.G. Barton, S.G. Podkolzin, J. Phys. Chem. B 109 (2005) 2262.
[88] M. Valden, X. Lai, D.W. Goodman, Science 281 (1998) 1647.
[89] M. Mavrikakis, P. Stoltze, J.K. Nørskov, Catal. Lett. 64 (2000) 101.
[90] N. López, T.V.W. Janssens, B.S. Clausen, Y. Xu, M. Mavrikakis, T. Bligaard, J.K. Nørskov, J. Catal. 223 (2004) 232.
[91] C. Lemire, R. Meyer, S. Shaikhutdinov, H.-J. Freund, Angew. Chem. Int. Ed. 43 (2004) 118.
[92] A. Corma, M. Boronat, S. González, F. Illas, Chem. Commun. (2007) 3371.
[93] H. Dyrbeck, N. Hammer, M. Rønning, E.A. Blekkan, Top. Catal. 45 (2007) 21.
[94] G. Mul, A. Zwijnenburg, B. van der Linden, M. Makkee, J. Moulijn, J. Catal. 201 (2001) 128.
[95] C. Sivadinarayana, T.V. Choudhary, L.L. Daemen, J. Eckert, D.W. Goodman, J. Am. Chem. Soc. 126 (2004) 38.
[96] B. Chowdhury, J.J. Bravo-Suárez, N. Mimura, J.Q. Lu, K.K. Bando, S. Tsubota, M. Haruta, J. Phys. Chem. B 110 (2006) 22995.
[97] J.T. Miller, A.J. Kropf, Y. Zha, J.R. Regalbuto, L. Delannoy, C. Louis, E. Bus, J.A. Van Bokhoven, J. Catal. 240 (2006) 222.
[98] I.N. Remediakis, N. López, J.K. Nørskov, Angew. Chem. Int. Ed. 44 (2005) 1824.
[99] L.M. Molina, M.D. Rasmussen, B. Hammer, J. Chem. Phys. 120 (2004) 7673.
[100] A. Zwijnenburg, M. Saleh, M. Makkee, J.A. Moulijn, Catal. Today 72 (2002) 59.
[101] A.L. de Oliveira, A. Wolf, F. Schüth, Catal. Lett. 73 (2001) 157.
[102] S.T. Oyama, X. Zhang, J.Q. Lu, Y. Gu, K.K. Bando, T. Fujitani, ACS Petr. Chem. Div. Prep. 52 (2007) 263.
[103] M. Okumura, Y. Kitagawa, K. Yamaguchi, T. Akita, S. Tsubota, M. Haruta, Chem. Lett. 32 (2003) 822.
[104] D.H. Wells, A.M. Joshi, W.N. Delgass, K.T. Thomson, J. Phys. Chem. B 110 (2006) 14627.
[105] J.Q. Lu, X. Zhang, J.J. Bravo-Suárez, S. Tsubota, J. Gaudet, S.T. Oyama, Catal. Today 123 (2007) 189.
[106] J.J. Bravo-Suárez, J.Q. Lu, C.G. Dallos, T. Fujitani, S.T. Oyama, J. Phys. Chem. C 111 (2007) 17427.
[107] J.J. Bravo-Suárez, K.K. Bando, J.Q. Lu, M. Haruta, T. Fujitani, S.T. Oyama, J. Phys. Chem. C 112 (2008) 1115.
[108] J.E. Rekoske, M.A. Barteau, J. Catal. 165 (1997) 57.
[109] E. Finocchio, G. Busca, V. Lorenzelli, R.J. Willey, J. Chem. Soc. Faraday Trans. 90 (1994) 3347.
[110] C.B. Khouw, C.B. Dartt, J.A. Labinger, M.E. Davis, J. Catal. 149 (1994) 195.
[111] K. Chen, A.T. Bell, E. Iglesia, J. Phys. Chem. B 104 (2000) 1292.